A&A 380, 19–30 (2001)
DOI: 10.1051/0004-6361:20011252

Astronomy & Astrophysics

Stellar populations in Seyfert 2 galaxies

I. Atlas of near-UV spectra⋆,⋆⋆

B. Joguet[1], D. Kunth[1], J. Melnick[2], R. Terlevich[3,⋆⋆⋆], and E. Terlevich[4,†]

[1] Institut d'Astrophysique de Paris, 98bis boulevard Arago, 75014 Paris, France
e-mail: kunth@iap.fr
[2] European Southern Observatory, Casilla 19001, Santiago 19, Chile
e-mail: jmelnick@eso.org
[3] Institute of Astronomy, Madingley Road, Cambridge CB3 0HA, UK
e-mail: rjt@ast.cam.ac.uk
[4] Instituto Nacional de Astrofísica, Óptica y Electrónica, Apdo. postal 25 y 216, 72000 Puebla, Pue., Mexico
e-mail: et@ast.cam.ac.uk

Received 4 April 2001 / Accepted 6 August 2001

Abstract. We have carried out a uniform spectroscopic survey of Seyfert 2 galaxies to study the stellar populations of the host galaxies. New spectra have been obtained for 79 Southern galaxies classified as Seyfert 2 galaxies, 7 normal galaxies, and 73 stars at a resolution of 2.2 Å over the wavelength region 3500–5300 Å. Cross-correlation between the stellar spectra is performed to group the individual observations into 44 synthesis standard spectra. The standard groups include a solar abundance sequence of spectral types from O5 to M3 for dwarfs, giants, and supergiants. Metal-rich and metal-weak F-K giants and dwarfs are also included. A comparison of the stellar data with previously published spectra is performed both with the individual spectra and the standard groups. For each galaxy, two distinct spatial regions are considered: the nucleus and the external bulge. Spectroscopic variations from one galaxy to another and from the central to the external region are briefly discussed. It is found that the central region of a Seyfert 2 galaxy, after subtracting the bulge stellar population, always shows a near-UV spectrum similar to one of three representative categories: a) many strong emission lines and only two visible absorption lines (Ca II K and G band) (Sey2e); b) few emission lines, many absorption lines, and a redder continuum than the previous category (Sey2a); c) an almost flat continuum and high-order Balmer lines seen in absorption (Sey2b). The proportion of Seyfert 2 galaxies belonging to each class is found to be 22%, 28%, and 50% respectively. We find no significative differences between morphology distributions of Seyfert 2 galaxies with Balmer lines detected in absorption and the rest of the sample. This quick look through the atlas indicates that half of Seyfert 2 galaxies harbour a young stellar population (about or less than 100 Myr) in their central region, clearly unveiled by the high order Balmer series seen in absorption.

Key words. atlases – galaxies: active – galaxies: Seyfert – galaxies: starburst – galaxies: stellar content

1. Introduction

Type 2 Seyfert nuclei are known to contain a "blue featureless continuum" (BFC) which gives a significant contribution in the optical and ultraviolet (UV). However, the nature of this BFC is not clear. Optical spectropolarimetry (Tran 1995a) shows that only a minor fraction of the BFC can be understood as scattered light from a hidden Seyfert 1 nucleus. Tran (1995b, 1995c) has also suggested, within the context of the standard model, that the BFC could be unpolarized thermal radiation from electron clouds within the ionization cones. However, Cid Fernandes & Terlevich (1995) argue convincingly that this BFC is associated with a young stellar population which is not obscured by the torus, is unpolarized, and therefore will heavily dilute the total polarization of any reflected nuclear component. This young stellar population could also account for the Ca II triplet absorption lines seen in Seyfert spectra which are as deep or even deeper than in normal galaxies and therefore are clearly not diluted by a non-stellar continuum (Terlevich et al. 1990). Heckman et al. (1995) have

Send offprint requests to: B. Joguet, e-mail: joguet@iap.fr
⋆ Based on observations collected at the European Southern Observatory, Chile (ESO 65.P-0014(A)).
⋆⋆ Tables 1–3 and 8 and Fig. A.1 (Appendix A) are only available in electronic form at http://www.edpsciences.org
⋆⋆⋆ Visiting Profesor at INAOE, Mexico.
† Visiting Fellow at IoA, UK.

confirmed this view in the UV spectral region ($\lambda\lambda$1200–1900). In addition, they have found that ∼30% of the Balmer emission lines might be powered by a starburst, and, finally, that the most likely explanation for the BFC is that a significant fraction is produced by a dusty circumnuclear population of massive stars which is unusually luminous compared to normal galaxies of the same Hubble type. Indeed, Colina et al. (1997) provided direct evidence that, for four galaxies having a Seyfert 2 type nucleus surrounded by a star-forming ring, the UV flux emitted is dominated by radiation coming from clusters of young hot stars distributed along the star-forming ring (the Seyfert nucleus' contribution amounts only to ∼1%–10% of the observed UV flux). González-Delgado et al. (1998) showed that the BFC is actually not featureless but contains stellar wind and photospheric lines in the UV, HeI and high-order Balmer absorption lines in the near-UV, and Ca II triplet lines in the near-IR. However, the galaxies were selected on the basis of the brightness of the nucleus in the UV, a criterion which could favor galaxies with more vigorous nuclear starbursts.

These results imply that starbursts play energetically significant roles in some active galaxies and suggest a possible causal relationship between Seyfert activity and starbursts since both phenomena are found to coexist even on small scales. Indeed, Heckman et al. (1997) demonstrated that a very compact starburst is occuring in the vicinity of the hidden Seyfert nucleus of MRK 477. Aretxaga et al. (2001) also observed strong Balmer absorption lines in two out of six luminous radiogalaxies, that they interpreted as signatures of massive stars. So, it is clear that AGN and starbursts commonly co-exist in the central regions of many Seyfert and radio galaxies.

Schmitt et al. (1999) performing spectral synthesis using six optical stellar absorption lines found that the 20 Seyfert 2 galaxies of their sample have a large contribution from stars with ages of 100 Myr. Storchi-Bergmann et al. (2000) used the same sample and focussed the analysis on the wavelength range $\lambda\lambda$3500−4100. They find signatures of stars younger than 500 Myr in six galaxies (30% of their sample). Boisson et al. (2000) observed 12 galaxies among which 3 are Seyfert 2 galaxies. They found that Seyfert 2 nuclei show a very metal rich young stellar component (∼10 Myr). González-Delgado et al. (2001) observed 20 bright Seyfert 2 galaxies from the near-UV to the near-IR and used Balmer and HeI absorption lines to model the stellar populations. They revealed that half of the nuclei harbor young stars (∼few×100 Myr). However, most samples were small, the largest one containing only 20 Seyfert 2 galaxies.

We have carried out a uniform spectroscopic survey of 79 catalogued Southern Seyfert 2 galaxies to study the stellar populations of the host galaxies, by means of near-UV and blue spectroscopy at medium spectral resolution (2.2 Å) and a good spatial resolution (0.82″). All data were obtained with the same telescope, UV-sensitive detector, and setup.

This paper is the first of a series presenting the results from these observations. In Sect. 2, the observations and data reduction processes are described in detail. Section 3 is dedicated to the stellar library built for stellar population synthesis purposes. Section 4 presents the galaxy spectra together with re-classification of the activity type when necessary and Sect. 5 presents the discussion.

2. Observations and data reduction

We have carried out spectroscopic observations of nearby Seyfert 2 galaxies in four observing runs between May 1998 and August 2000, with the 1.52 m ESO telescope, at La Silla (European Southern Observatory – Chile).

We used the Boller & Chivens spectrograph equipped with a 2048 × 2048 pixel CCD camera with a spatial sampling of 0.82″ per pixel. A UV blazed grating of 1200 lines/mm with a dispersion of 0.98 Å per pixel was used. This CCD is ideally suited for our observations since it has a particularly high quantum efficiency below 5000 Å. However, this high quantum efficiency in the blue and UV is obtained via the backside passivation treatment called "UV flooding" which slightly degrades the spectral resolution because electrons created in the field-free region may drift into neighbouring cells. For this reason the spectral resolution is 2.2 Å *FWHM* for a 1.5″ wide slit.

During the observations of both galaxies and stars, we took special care to minimize the effect of atmospheric differential refraction by observing at paralactic angle and low airmass.

The data reduction was carried out using the ESO-MIDAS package. Standard reduction procedures for bias subtraction, bad pixel correction, and flat-fielding were applied. Most observations of galaxies were performed taking three 20 min spectra in order to cleanly remove the cosmic rays. Rebinning flux onto a linear wavelength scale was done row by row, using the spectrum of helium/argon calibration lamp observed just before or just after each exposure. Sky subtraction was then performed. By measuring the sky levels in frames of stars and because we were only considering the central 280 columns that cover the full slit length (4.5′), we determined that there was no significant vignetting along the spatial direction. The final sky spectrum was obtained by averaging 25″ (30 pixels) on both sides of the galaxies, not too far from the sampled regions. The data were then corrected for airmass using the La Silla extinction curve measured by Tüg from 1974 to 1976 (Tüg 1976). Finally, flux calibration was performed using three to five spectrophotometric standard stars observed each night.

3. Stellar data

3.1. The stellar sample

We selected a sample of stars covering the *HR* diagram putting particular emphasis on massive stars.

The list of observed stars is given in Table 1. The spectral types are from SIMBAD, i.e. various sources in the literature.

The mass estimates come from Table 23 in Schmidt-Kaler (1982) for the stars with spectral types later than A5 and from Mas-Hesse & Kunth (1991) for stars younger than A5.

The reddenings $E(B-V) = (B-V) - (B-V)_0$ are computed using the intrinsic colors given in Table 1 of Fitzgerald (1970) using the spectral types and the observed colors given in the literature. The reddening distribution has a mean of 0.14 and a standard deviation of 0.26 assuring that the stellar spectra are relatively independent of our choice of reddening law; we used the galactic reddening law determined by Cardelli et al. (1989) with $R_V = 3.2$. Errors introduced from reddening corrections are estimated to be about 5% at most.

The metallicities are taken from Cayrel de Strobel (1997), Leitherer et al. (1996), or the compilation made by Taylor (1999). Stars with no published metallicities are assumed to have a solar value although some of them have $|b| > 20°$ indicating that they could belong to the Galactic halo and be metal-poor stars (HD 28099, HD 30739, HD 15318, HD 185467, HD 196917, HD 188352, HD 188088, HD 181321, HD 213998, HD 8779).

3.2. A composite library

In order to avoid degeneration in our stellar library, i.e. the fact that two stellar templates contain the same information in terms of equivalent widths and continuum slopes, we decided to group individual spectra with similar temperature, abundance, and gravity (TZG) parameters. An additional advantage is that such groupings are much more representative of their associated TZG since they depend less on peculiar spectral properties of individual stars.

The self-comparison of dereddened stellar spectra was performed through cross-correlation from 3500 to 5300 Å. For this, we used the software library RVSAO 2.0 (Kurtz & Mink 1998) running under IRAF. This method only uses the information contained in spectral features, therefore possible color and reddening residuals do not affect the results. We used as similarity criterion the function defined by Tonry & Davis (1979):

$$r = \frac{h}{\sqrt{2}\sigma_{\rm a}}, \quad (1)$$

where h is the correlation peak height and $\sigma_{\rm a}$ is the standard deviation of the antisymmetrical component of the correlation function. If spectra are identical, the correlation function is symmetrical and $\sigma_{\rm a} = 0$. Practically, $\sigma_{\rm a} \neq 0$ but the most similar the spectra are, the smaller $\sigma_{\rm a}$ is, while h increases, i.e. the higher r is. An advantage of this method is that, in opposition to h, r takes into account the signal-to-noise ratio of the convolved spectra through $\sigma_{\rm a}$.

We first cross-correlated individual spectra of stars for which several spectra had been obtained. The r distribution was found to vary from 50 to 1015 with a mean at 217. Therefore, we decided to apply the following likeness criterion of spectra: $r \geq 50$.

This method allowed us to group individual spectra of stars with similar spectral types but the distinction between luminosity classes turned out to be more difficult, especially for young stars. In fact, we used both likeness criterion and TZG values given in the literature to build the standard groups.

Finally, individual spectra with close TZGs have been averaged according to the compositions given in Table 2. In this way, systematic effects such as inconsistent TZG determinations or spectrophotometric calibration errors are reduced. Flux points more than 3σ away from the mean value have been rejected and final spectra have been normalized to 1 at 4020 Å.

Resulting spectra are shown in Fig. 1 while the HR diagram coverage of the final standard groups is presented in Fig. 2. According to spectral types and luminosity classes, absolute magnitudes are taken from Lequeux (2000).

3.3. Comparison with the literature

Consistency tests were performed using inter-library comparisons. Four published stellar libraries are available with spectral resolution higher than 15 Å, a good coverage of the TZG parameter space, and an overlap with our wavelength coverage:

- Jacoby et al. (1984) (JC84 hereafter);
- Pickles (1985);
- Silva & Cornell (1992) (SC92 hereafter);
- Jones (1997) (J97 hereafter).

SC92 have shown that the spectrophotometric accuracy of the Pickles' library is very poor below 4000 Å what makes meaningless any comparison with these spectra.

In order to compare our stellar data with JC84 several preliminary steps are necessary. Because JC84 spectra are from individual stars, we selected appropriate stars from their library, averaged their spectra, and normalised to 1 at 4020 Å. At the same time, we smoothed with a Gaussian function and resampled our data in order to bring them to the spectral resolution and sampling as JC84 spectra.

Comparison between composite spectra built from JC84 and their analogues from our library gives both well- and poorly-matched results. The best two agreements are shown in Figs. 3a–d. Figures 3a and b show our standard group B0.5III compared with the B1III star HD 13494 from JC84. In Figs. 3c and d, our standard group F0V is compared with the F0V star HD 10032 from JC84.

Spectral residuals are defined by:

$$R_i = 1.0 - \frac{JC84_i}{\mathrm{OurData}_i},$$

where i refers to every running pixel.

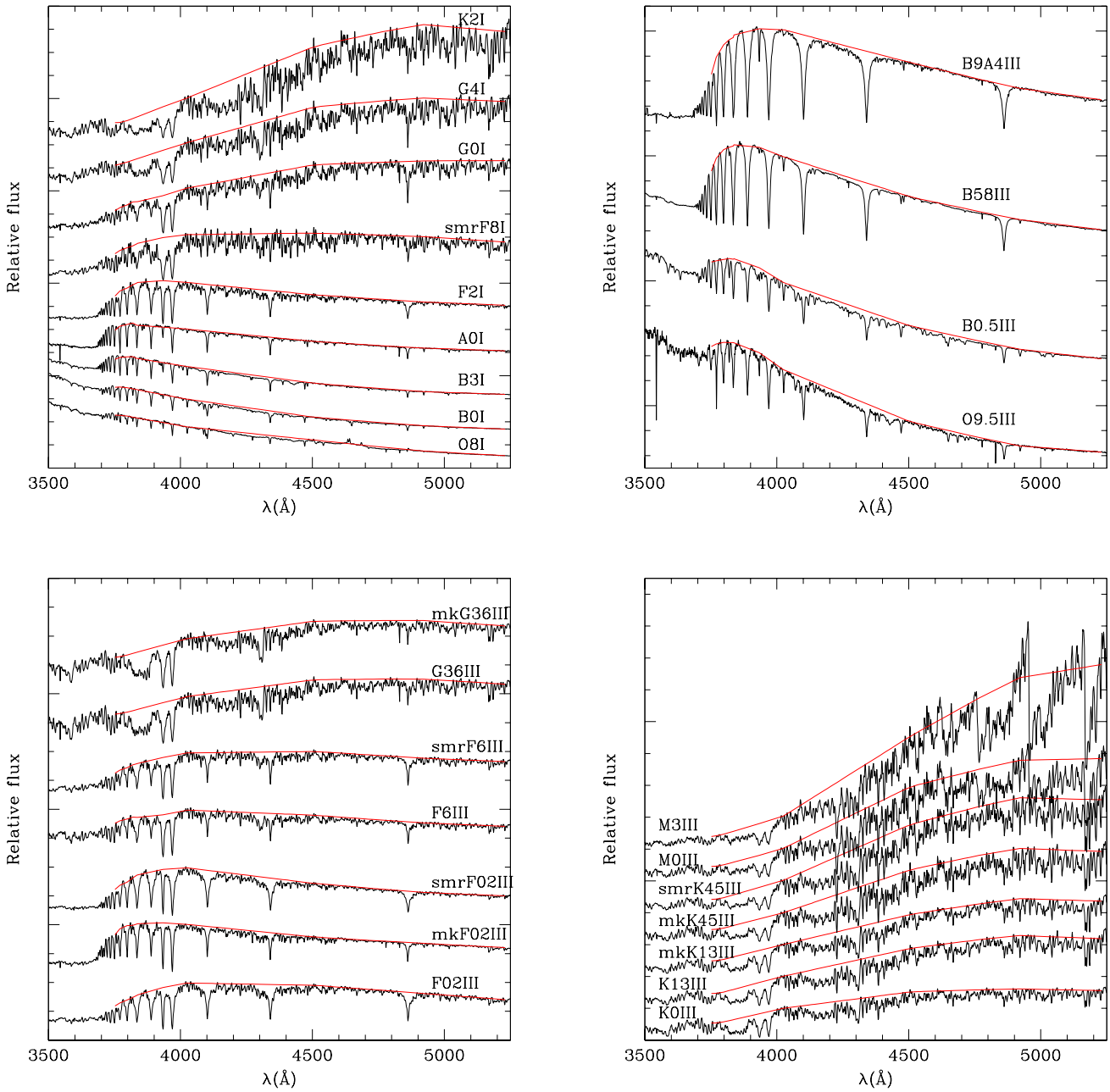

Fig. 1. Spectra of stellar groups ordered by spectral types. Each spectrum has been normalized to 1 at 4020 Å and a constant added when necessary. The continuum fit used for *EW* measurements is superimposed on each spectrum.

The worst matched spectra are shown in Figs. 3e–h. Figures 3e and f show our standard group O9V compared with the O9V stars HD 17520 and HD 12323 from JC84. In Figs. 3g and h, our standard group F8Iab is compared with the F8Ib star HD 187428 from JC84.

Following the same procedure, we then compared our standard groups with the composite library SC92.

The best-matched two spectra are displayed in Figs. 4a–d while the worst-matched two spectra are shown in Figs. 4e–h. The compared standard groups from both libraries are given in the figures.

High-frequency differences are certainly due to a combination of spectral resolution differences, wavelength calibration shifts, and intrinsic physical differences between the stars actually observed. All continua differences can be explained by spectrophotometric calibration and dereddening differences (5% at most) since the observed residuals have the same order of magnitude as the residuals presented in Figs. 9 and 10 of SC92. Given the estimated spectrophotometric accuracy of our data (10%), there is no way of assessing which dataset is less accurate than another.

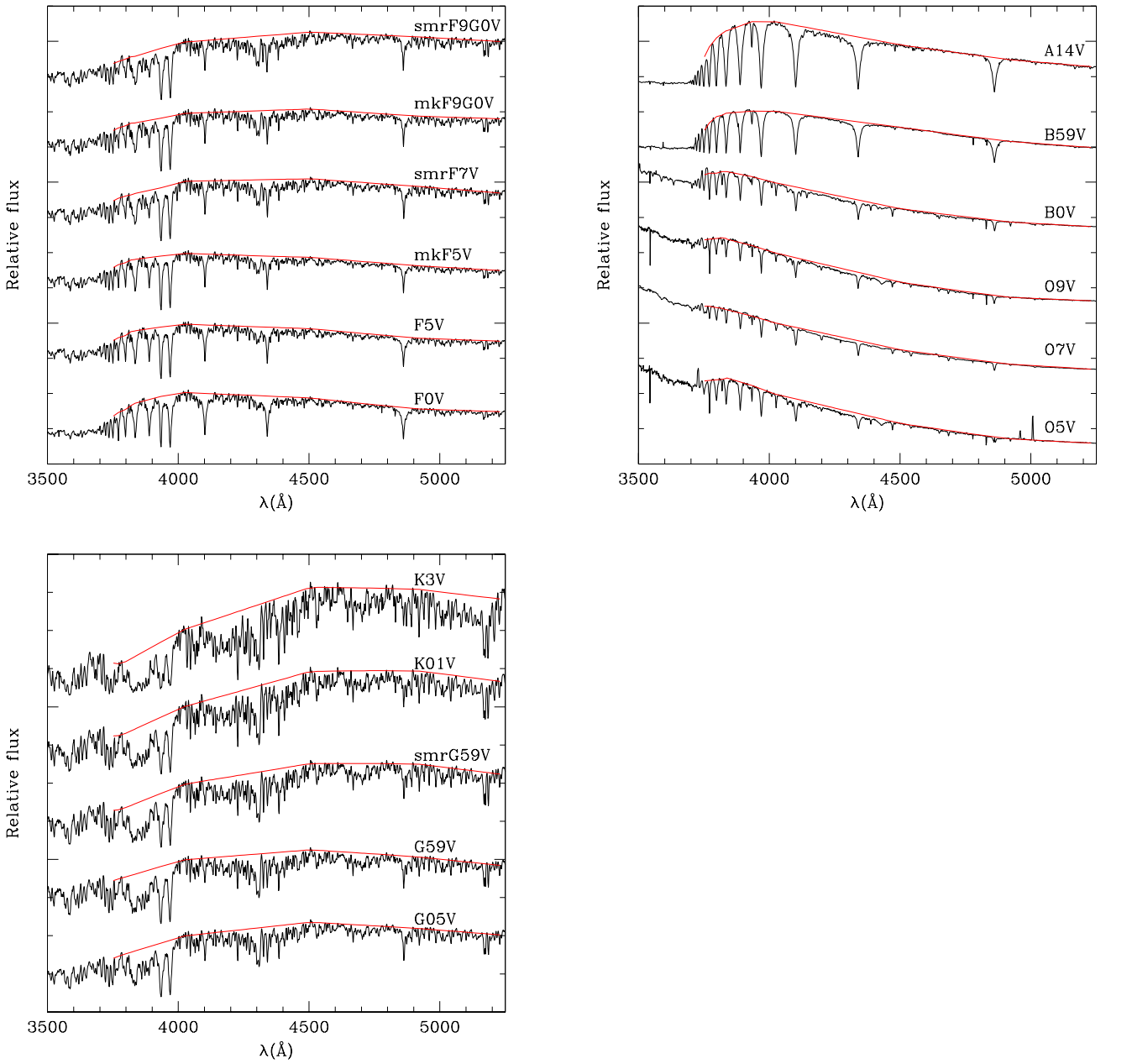

Fig. 1. continued.

The final comparison is performed directly with the individual spectra. Indeed, among the observed stars, 30 were also observed by J97. Unfortunately the wavelength range is not fully covered and the spectra were not flux-calibrated by J97. However, we compared the measurements of 29 indices obtained for each individual spectrum with those previously published (Leitherer et al. 1996). For this, we strictly followed the method described by Worthey et al. (1994) using the definitions of indices given in Worthey et al. (1994) and Rose (1994). We find no significative trend norsystematic bias between measurements inside a dispersion of about 10% for indices measured in Å and about 0.03 mag for those measured in magnitudes.

In summary, by comparing our stellar data with previously published stellar libraries, we have shown that our standard groups are reasonably well flux-calibrated and reproduce previous measurements of spectral properties. This stellar library offers a good sampling of the HR diagram and covers metallicities, [Fe/H], from −1.10 to +0.80.

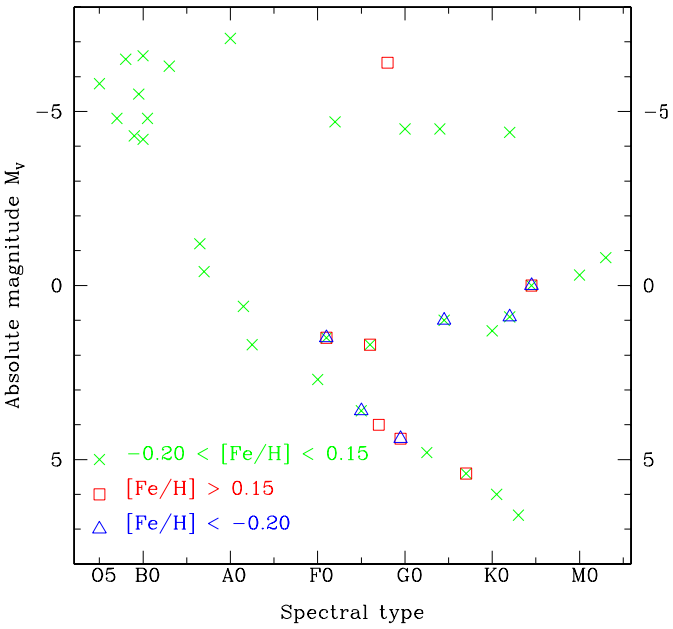

Fig. 2. *HR* diagram of the standard groups included in the composite stellar library.

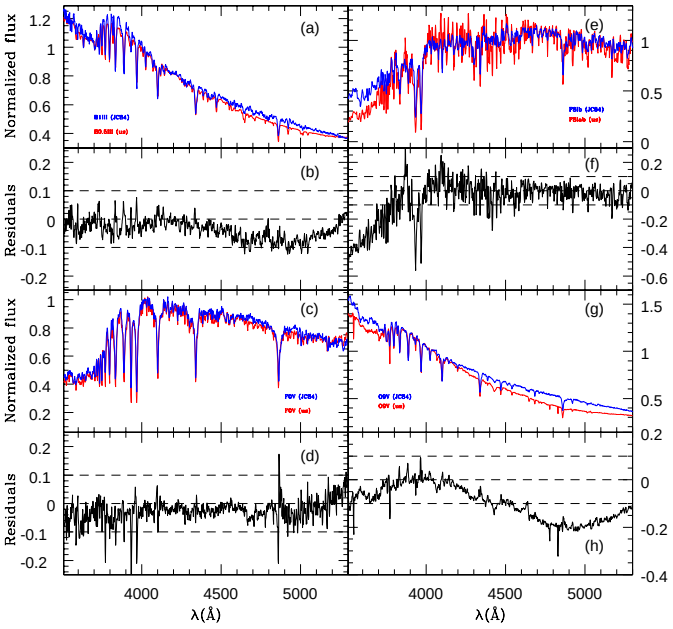

Fig. 3. Comparison between JC84 and our data: well-matched (left side) and poorly-matched (right side) spectra. **a)**, **c)**, **e)**, and **g)** Our data are compared with JC84. Spectra are normalized to 1 at 4020 Å. **b)**, **d)**, **f)**, and **h)** Negative residuals indicate that our composite spectrum has less relative flux at that point than the comparison JC84 star.

4. The galaxy sample

The sample was obtained from three catalogues of AGNs: Fairall et al. (1991, hereafter F91), Lipovetsky et al. (1988, hereafter L88), and Véron-Cetty et al. (1998, hereafter V98). The selection criteria were defined as follows:

– Galaxy classified as Seyfert 2 in at least one of the three catalogues;

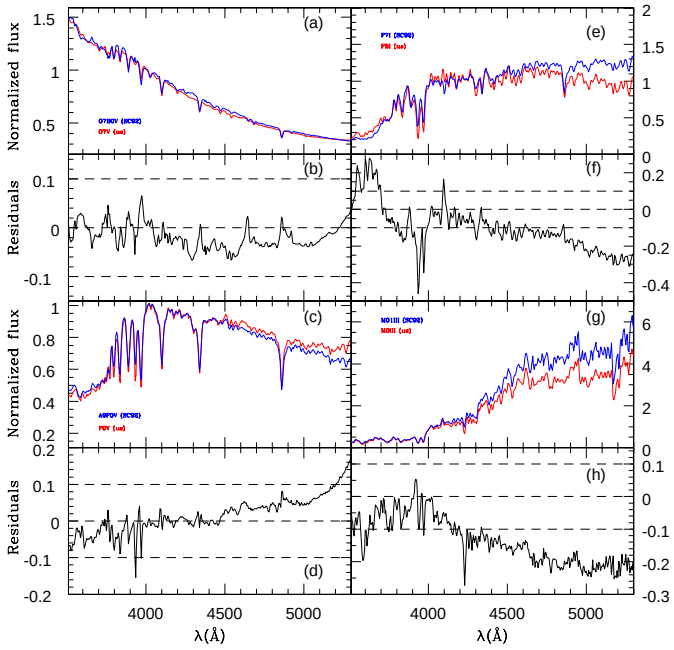

Fig. 4. Same as Fig. 3 but the comparison in now performed between SC92 and our data.

– Galaxy observable from La Silla (Chile), i.e. with $-67° < \delta < +15°$;
– Nearby galaxy: $0.002 < z \leq 0.017$.

Only one galaxy was found to be at $z < 0.002$, NGC 4945. We removed it from the sample since, given the field size of the CCD and the spatial extension of the host galaxy, it was not possible to correctly subtract the sky emission from the spectrum.

The resulting sample contains 71 galaxies out of 959 from L88, 73 galaxies out of 4428 from V98, and 44 galaxies out of 12 844 from F91. After merging, the whole sample has 106 Seyfert 2 galaxies.

However, because of weather and observability constraints, only 74 galaxies (70%) could be observed. Computing the completeness distribution over redshift and V magnitude, we have checked that still this sample can be considered as a distance-limited sample with $cz \leq 5100\ \mathrm{km\,s^{-1}}$. Relaxing somehow the proximity constraint, 8 more Seyfert 2 galaxies were observed (NGC 3362, NGC 5252, MRK 1370, NGC 5674, MRK 883, MRK 897, Fairall 334, and NGC 7212). They were chosen as well-studied and bright Seyfert 2 galaxies and were added to the original sample to allow more comparisons with literature. We consider them as part of the final sample since they only represent 10% of the total sample size and should not significantly modify our results.

Additional galaxies for comparison have been observed: 7 with different morphologies (from ellipticals to late-type spirals) and no activity, 3 Seyfert 1 galaxies, 3 LINERs, and 4 Seyfert 1.9 galaxies. All comparison galaxies have been chosen within the same redshift range as our programme galaxies in order to maintain the same spatial resolution in the galaxies.

The journal of observations is given in Table 3 and the radial velocity distribution of the sample is given in Fig. 5.

We performed spatial extractions of the nuclear and external regions of each galaxy. We assumed that the external regions had the same overall stellar population at both sides of the nucleus and therefore we added both external extractions. In a forthcoming paper (Joguet et al. 2001b) we will present the spatially resolved data extracted row by row from the 2D spectra in order to follow spatial gradients and asymmetries in the stellar and dust content of the host galaxies.

The spatial regions on which data were averaged to build up the 1D spectra are given in the Appendix (Fig. A.1). Two light profiles are given for each galaxy: the dotted line corresponds to the light emitted in the [O III] λ5007 emission line and traces H II regions and high ionization regions in the galaxy while the full line corresponds to the stellar continuum emitted between 4000 and 4100 Å. Fluxes have been normalized at the maximum.

Both light profiles are similar except for those cases where the ionized regions tend to be more compact than the bulge of the host galaxy (NGC 3081, NGC 4388, NGC 5506, NGC 5427, NGC 6890, NGC 7314, NGC 1125, NGC 1667, NGC 3362, ESO 383G18, and NGC 3281).

Resulting nuclear and external 1D spectra are given in the Appendix (Fig. A.1).

At first glance it is difficult to precisely estimate the level of activity in each individual galaxy since a) we do not cover a wide range in wavelength; in particular we do not have any information on Hα, [N II], and [S II] emission fluxes so we cannot use well-established diagnostic diagrams (Baldwin et al. 1981) and b) we must first subtract the stellar component before measuring the emission-line fluxes. This requires a detailed analysis that will be carried out in a following paper (Joguet et al. 2001b).

One extreme example of such ambiguous classification between starburst galaxy, LINER and Seyfert 2 galaxy is NGC 7496. From its optical spectrum, one may be tempted to consider this galaxy as a starburst galaxy. However, it has hard X-ray emission, and therefore harbours a Seyfert nucleus.

4.1. Misclassified galaxies

Our sample was defined based on previous observations performed under various technical conditions; in our homogeneous observations, some of them show spectra different from a classical Seyfert 2 galaxy. Their central region spectra were analyzed. Table 4 gives the physical regions on which the spectra were summed up (we adopted $H_0 = 80$ km s^{-1} Mpc^{-1}) and Table 5 gives the emission line fluxes relative to Hβ without reddening correction, together with the *FWHM* of the fitted Gaussian profiles. Table 6 summarizes the classification changes.

Three galaxies in the sample turned out to be starburst galaxies with Wolf-Rayet (WR) stars revealed by broad emission lines around He II λ4686. Their continuum slope is particularly blue and very weak. All the Balmer series is seen in strong emission while higher ionization emission lines are weaker. **IC 4870** had been previously classified as a starburst (Whittle 1992) although Véron (1981) identified it as a Seyfert 2 galaxy. **IC 5154**, and **ESO 108G17** are still mentioned as Seyfert 2 galaxies in Véron et al. (2000) who take this classification from Allen et al. (1991) although Schaerer et al. (1999) had already reported this misclassification. **IC 5154** has an irregular morphology with two bright nuclei (IC 5154a and IC 5154b correspond to the South-East and North-West spots, respectively). The WR line fluxes are listed separately in Table 7 for the sake of clarity. A following paper will be entirely devoted to the full description and analysis of these three WR galaxies (Joguet et al. 2001a).

NGC 7135 barely shows [O III] emission lines: EW([O III]5007) = -0.7 Å. Our spectrum is in agreement with the Fig. 6b in Longhetti et al. (1998), supporting the view that this galaxy is rather an early-type galaxy with no active nucleus: only a weak Hβ emission line is observed while several strong stellar absorption features are visible.

NGC 7410 shows weak [O III] emission lines: EW([O III]5007) = -1.8 Å. Vaceli et al. (1997) observed this galaxy in May 1991 and classified it as a LINER (Low Ionization Nuclear Emission-line Region), using diagnostic diagrams (Baldwin et al. 1981) built with emission-line intensities obtained after stellar population subtraction.

ESO 508G05 does not show any emission lines.

NGC 7811 shows broad Hδ and Hγ emission lines without narrow components. The Fe II emission bump is clearly visible around 4570 Å with $EW = -42$ Å. Hβ can be fitted by two components (narrow and broad centered at the same position). Values obtained in Table 5 confirm that **NGC 7811** is a Seyfert 1.5 galaxy.

NGC 1365 shows two flux maxima along the slit. This led to two extractions as shown in Table 4. The measured values for the *a* extraction clearly indicate that **NGC 1365** is a Seyfert 1.5 galaxy.

NGC 3035 is a misclassified Seyfert 1 galaxy. Its spectrum is very similar to that of NGC 4903, a classical Seyfert 2 galaxy. No broad emission line is seen while [O III] λ5007, Hβ, [O II] λ3727, and [Ne III] λ3870 and several strong stellar absorption features are present (Ca II H and K, CH band, Mg I$\lambda\lambda$5170, 5184). However, variability could be an explanation for such unexpected spectroscopic properties. Indeed, when the obscuring medium is along our line-of-sight to the central engine, the AGN disappears while the starlight becomes the dominant component of the spectrum: then, strong absorption features would be expected together with emission lines from the ionized gas in the narrow line region. Conversely, when the AGN shows up, its strong blue continuum would dilute all absorption lines and broad emission lines would appear.

NGC 7314 has a spectrum and line fluxes typical of a Seyfert 2 galaxy. Therefore we exclude the classification of Seyfert 1. However, variability of the Seyfert nucleus

Table 4. Physical regions (in $''$ and kpc) considered for the activity classification and line flux measurements.

IC4870	IC5154a	IC5154b	E108G17	N7314	N1365a	N1365b	N3035	N7811
2.4×2	4.8×2	4×2	2.4×2	2.4×1.5	7.2×1.5	6.4×1.5	2.4×1.5	2.4×1.5
0.14×0.1	1×0.4	0.8×0.4	0.3×0.3	0.2×0.1	0.7×0.2	0.7×0.2	0.7×0.4	1.2×0.8

Table 5. Emission line parameters of the misclassified galaxies : for each galaxy, the first value is the $FWHM$ ($\mathrm{km\,s^{-1}}$) and the second column is the intensity relative to $I(\mathrm{H}\beta\mathrm{n}) = 100$.

Line	IC4870	IC5154a	IC5154b	E108G17	N7314	N1365a	N1365b	N3035	N7811
[O II] λ3727	440 51.8 ± 2	450 266. ± 5	440 198 ± 5	440 264. ± 5	400 197 ± 5	440 55.1 ± 2	370 92 ± 2	540 333 ± 5	– –
H_{12}	160 1.1 ± .2	– –	210 1.2 ± .2	180 1.4 ± .2	– –	– –	– –	– –	– –
H_{11}	160 1.1 ± .2	– –	230 2.1 ± .3	180 1.6 ± .2	– –	– –	– –	– –	– –
H_{10}	180 2.5 ± .3	– –	220 2.9 ± .3	180 2.5 ± .3	– –	– –	– –	– –	– –
He I λ3819	– –	– –	– –	250 1.1 ± .2	– –	– –	– –	– –	– –
H_9	220 3.6 ± .3	150 2.1 ± .2	230 4.7 ± .3	210 4.6 ± .3	220 29 ± .5	– –	– –	– –	– –
[Ne III] λ3870	260 39.7 ± .5	270 16.5 ± .3	270 15.9 ± .3	260 19.3 ± .3	290 119 ± 1	360 22.9 ± .5	– –	470 192 ± 2	– –
HeI+H_8 λ3888	230 14.0 ± .3	210 11. ± .3	250 14.3 ± .3	240 15.1 ± .3	– –	230 5.3 ± .3	– –	– –	– –
[Ne III] λ3967	190 11.5 ± .3	– –	– –	– –	– –	– –	– –	– –	– –
Hϵ+HeII λ3970	190 11.5 ± .3	250 9.8 ± .3	330 16.0 ± .3	290 15.4 ± .3	310 35 ± .5	– –	– –	– –	– –
He I λ4026	220 1.6 ± .2	– –	210 1.3 ± .2	250 1.0 ± .2	– –	– –	– –	– –	– –
[S II] λ4068	– –	– –	280 1.8 ± .2	180 1.2 ± .2	– –	– –	– –	– –	– –
Hδ	220 19.7 ± .3	190 16.5 ± .3	230 21.3 ± .3	210 2.6 ± .3	– –	240 10.2 ± .3	– –	– –	4020 1007 ± 10
Hγ	220 42.0 ± 1	190 37.8 ± .3	230 41.9 ± .5	210 2.3 ± .3	840 81 ± 1	300 29.8 ± .3	– –	– –	3370 1393 ± 10
[O III] λ4363	210 8.7 ± .3	– –	280 1.8 ± .3	250 2.7 ± .3	610 55 ± .5	420 5.7 ± .3	– –	– –	– –
He I λ4388	230 0.9 ± .2	– –	– –	– –	– –	– –	– –	– –	– –
He I λ4471	210 3.6 ± .3	280 4.9 ± .2	150 6.4 ± .3	210 3.6 ± .3	– –	– –	– –	– –	– –
Fe II λ4560 b	– –	– –	– –	– –	– –	12430 245 ± 5	– –	– –	16610 3107 ± 10
[Fe III] λ4658	– –	280 2.4 ± .3	190 0.9 ± .2	– –	– –	– –	– –	– –	– –
He II λ4686	1680 17.4 ± .3	120 3.0 ± .3	120 3.4 ± .3	– –	260 45 ± .5	310 18.4 ± .3	– –	– –	– –
Hβn	220 100.	200 100.	220 100.	200 100.	270 100.	310 100.	250 100.	200 100.	170 100.
Hβb	– –	– –	– –	– –	– –	1790 85 ± 5	– –	– –	3000 1873 ± 15
He I λ4922	310 1.1 ± .2	– –	200 1.0 ± .2	120 0.6 ± .2	– –	– –	– –	– –	– –
[O III] λ4959	220 225 ± 5	200 87.2 ± 1	210 102 ± 2	200 112 ± 2	280 487 ± 5	300 75 ± 2	300 17 ± .3	300 729 ± 5	390 353 ± 5
[Fe III] λ4987	– –	120 1.2 ± .2	250 1.0 ± .2	180 0.9 ± .2	– –	– –	– –	– –	– –
[O III] λ5007	220 681 ± 5	200 266 ± 5	230 301 ± 5	200 335 ± 5	290 1571 ± 10	320 243 ± 3	310 65 ± 1	310 2250 ± 10	350 1033 ± 10
He I λ5016	– –	– –	250 9.5 ± .3	250 7.1 ± .3	– –	– –	– –	– –	– –
[N I] λ5200	– –	– –	250 1.0 ± .2	250 1.0 ± .2	– –	320 9.4 ± .3	390 40 ± .5	300 100 ± 1	– –

Table 6. Classification revision.

Galaxy	Previous classification	New classification
IC 4870	Seyfert 2	WR galaxy
IC 5154	Seyfert 2	WR galaxy
ESO 108-G17	Seyfert 2	WR galaxy
NGC 7410	Seyfert 2	LINER
NGC 7135	Seyfert 2	No activity
ESO 508-G05	Seyfert 2	No activity
NGC 1365	Seyfert 1.8	Seyfert 1.5
NGC 7811	Seyfert 1	Seyfert 1.5
NGC 3035	Seyfert 1	Seyfert 2
NGC 7314	Seyfert 1	Seyfert 2

Table 7. Wolf-Rayet features of the misclassified galaxies: for each galaxy, the first value is the $FWHM$ ($\mathrm{km\,s^{-1}}$) and the second column is the intensity relative to $I(\mathrm{H}\beta) = 100$.

Line identification	IC 4870	IC 5154b	E108G17
N III λ4640	400 0.7 ± .2	– –	– –
[Fe III] λ4658	400 0.9 ± .2	260 1.1 ± .1	210 1.3 ± .1
C IV λ4658	8000 13.5 ± .5	3520 6.3 ± .3	3070 7.5 ± .5
He II λ4686 n	400 2.3 ± .1	– –	500 0.5 ± .2
He II λ4686 b	1550 12.0 ± .3	925 4.3 ± .2	1470 3.8 ± .3
[Ar IV] λ4711	400 1.5 ± .1	400 1.0 ± .2	250 0.4 ± .1
[Ar IV] λ4740	260 0.6 ± .1	350 0.4 ± .2	– –

might explain the absence of broad emission lines, like in the case of **NGC 3035**.

4.2. Stellar kinematics of the galaxy sample

Stellar velocity dispersions have been obtained through cross-correlation between the 1D extracted galactic spectra and the standard groups built in Sect. 3. The cross-correlation was performed on the wavelength domain between 3980 and 4600 Å in order to avoid the Ca II H and K lines below 3980 Å which are known to severely bias the stellar velocity dispersion measurements and because most absorption features are present in this range. For each galaxy, all standard groups have been cross-correlated with the RVSAO 2.0 software and, again, the

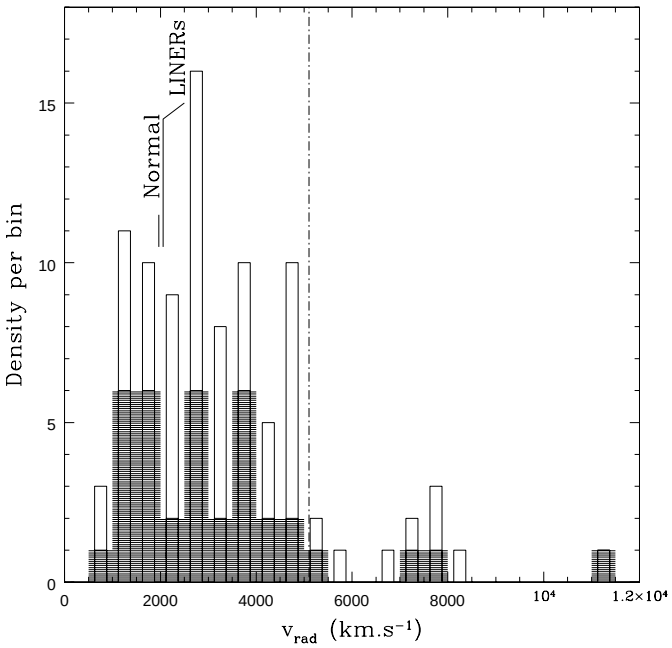

Fig. 5. Expansion velocity distribution of the sample of Seyfert 2 galaxies. Empty bars represent the whole sample while dashed bars only correspond to galaxies with Balmer lines detected in absorption. Mean radial velocities for the template galaxies and the LINERs are also indicated together with the completeness limit at 5100 km s^{-1}.

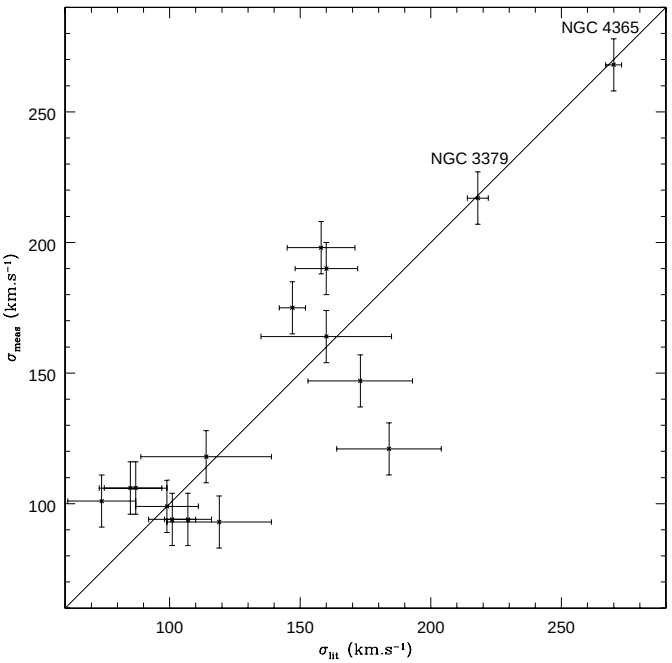

Fig. 6. Comparison between stellar velocity dispersions from the literature and our measurements.

correlation quality was estimated thanks to the r function (see (1)). We arbitrarily considered only correlations for which the r value was higher than 5 because for lower values the main correlation peak height becomes comparable to secondary peak heights. A weighted mean of final σs was then computed.

A comparison is performed between stellar velocity dispersions already published in the literature (Whitmore et al. 1985; Terlevich et al. 1990; Davoust et al. 1985; Nelson & Whittle 1995) and our measurements. The result is shown in Fig. 6. Although few galaxies show disagreements between both measurements, we do not see any bias between both estimates, from 100 to 280 km s^{-1}, especially when considering the "standard" galaxies as defined by Whitmore et al. (1985), i.e. the galaxies for which the central stellar velocity dispersion is known with high accuracy (NGC 3379 and NGC 4365).

5. Discussion

In this section, we consider only the central $2'' \times 2''$ region spectra of the sample galaxies.

5.1. Bulge subtraction

We have performed a bulge subtraction using seven templates scaled as to cancel the G-band absorption of the galaxies. So that the signal-to-noise ratio remains high enough, we smoothed all Seyfert 2 spectra over 3 pixels thus decreasing the spectral resolution from 1 Å to 3 Å per pixel. At such a low spectral resolution, differences in velocity dispersion of the stars in the template galaxies and in the Seyfert 2 galaxies do not show up any more: no further corrections were needed.

The G-band absorption is prominent in stars of spectral types later than F5 and it is particularly strong in K stars. Thus by subtracting G-band scaled templates of spiral and elliptical galaxies, we are isolating the most massive stars ($M > 1\ M_{\odot}$) in the composite stellar population of the central regions of the Seyfert 2 galaxies.

We used each template alone and gave priority to the template galaxy which had the same Hubble type as the Seyfert 2 galaxy considered when several templates were giving similar results. The template and Seyfert spectra were normalized at 4010 Å, and then progressive amounts of several different templates were subtracted from each Seyfert 2 galaxy until the remaining spectrum was relatively flat across the Ca II K line and the G band. This exercise in removing the starlight proved to be difficult. Often when an acceptable match was made in the $\lambda\lambda$3900−4300 region, the corrected spectrum diverged considerably in the red and over/under subtraction of MgI $\lambda\lambda$5174, 5184 showed up, presumably due to differences in the internal reddening and stellar content between the Seyferts and the templates. Note that no attempt was made to correct for internal reddening. The best corrected Seyfert spectrum was retained.

Table 8 presents for each galaxy the adopted best-fit template, and the derived fraction of stellar light coming from the bulge, f_*, near 4300 Å. The uncertainty in f_* is estimated to be ∼0.05. Figure 7 gives both distributions of f_* for the whole sample and the subsample including only Seyfert 2 galaxies with Balmer lines detected

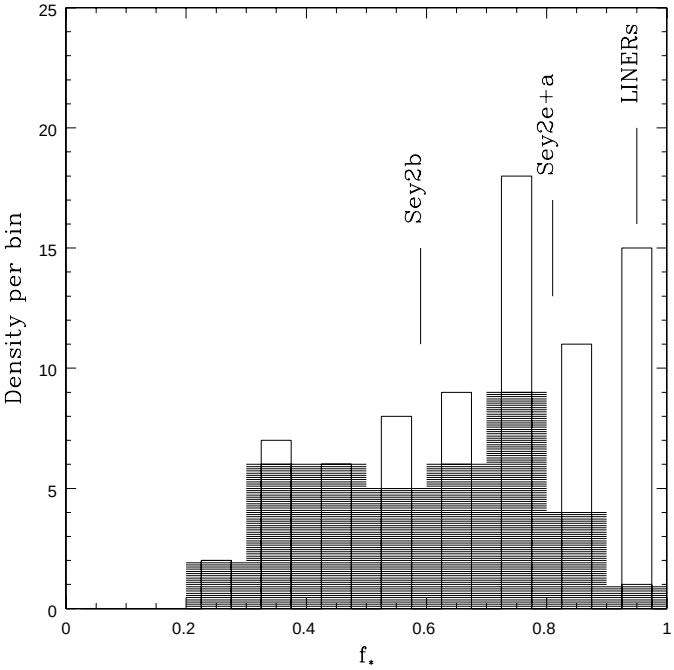

Fig. 7. Distribution of the fraction of stellar light, f_* coming from the bulge at 4300 Å. Empty bars represent the whole sample while the dashed bars count the galaxies with Balmer lines detected in absorption. Distribution means are 0.59 and 0.81 respectively, hence showing that galaxies with Balmer lines detected in absorption tend to have a smaller bulge stellar component or, conversely, that they tend to have a larger blue continuum than galaxies without young stellar population in their central region. The mean value obtained for the LINERs is also indicated.

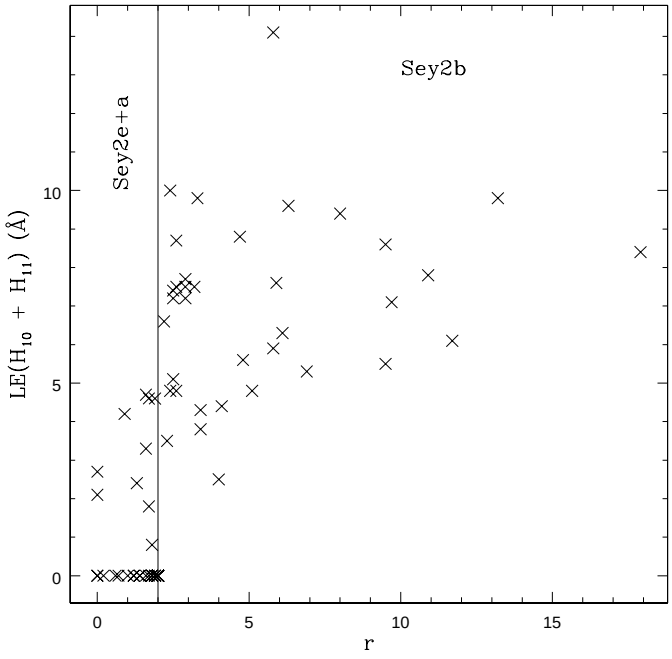

Fig. 8. Calibration of the detection limit of Balmer lines seen in absorption. Measured $EW(H_{10}+H_{11})$ are shown versus r. When $H_{10}+H_{11}$ are in emission, the EW is set to zero.

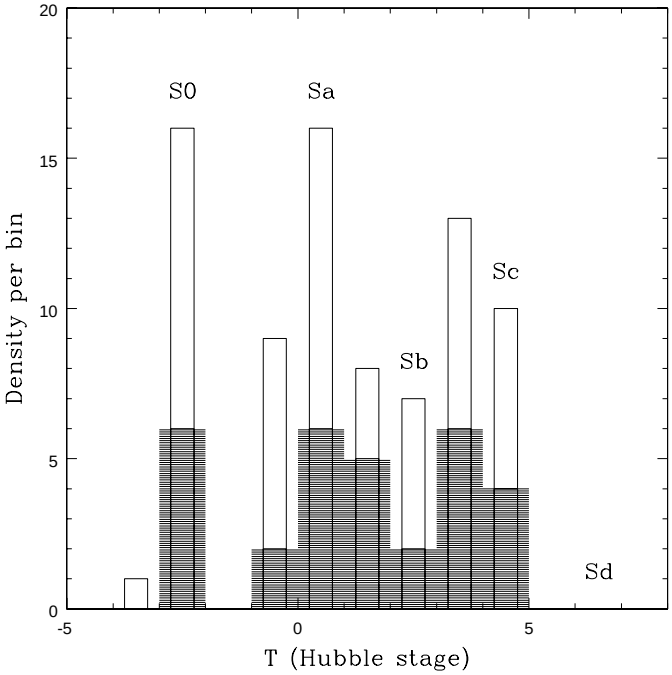

Fig. 9. Morphology distribution of the sample of Seyfert 2 galaxies: blank bars represent the whole sample while shaded bars count the galaxies with Balmer lines detected in absorption. The morphology comes from RC3.

in absorption. Distribution means are 0.59 and 0.81 respectively, thus indicating that galaxies with Balmer lines detected in absorption tend to have a weaker bulge component (conversely a larger blue continuum) than galaxies without young stellar population in their central region. A Student's t test performed on both distributions indicated that the probability that they are different is 53%.

Such a result is expected since the continuum emitted by young stars is almost featureless at 4300 Å and will dilute other absorption features formed by older stars in the bulge component.

5.2. Detection of high-order Balmer series in absorption

To provide a quantitative estimate of the fraction of light associated with Balmer absorptions, we performed a cross-correlation between each bulge-subtracted spectrum and the spectrum of an A0Ia star. Spectra were cross-correlated over the wavelength range $\lambda\lambda$3670–4000, after clipping the emission lines. We then sorted the galaxies according to increasing values of r (see (1)) and measured two Balmer absorption features, H_{10} λ3798 and H_{11} λ3770, fitting by hand single Gaussian profiles. Figure 8 represents the measured $EW(H_{10}+H_{11})$ versus r.

Based upon this figure, we decide that we detect high order Balmer series in absorption in all galaxies with $r \geq 2$, i.e. in 37 (50%) galaxies of the sample.

5.3. A rough classification of Seyfert 2 galaxies according to the nuclear stellar activity

We have grouped the Seyfert 2 galaxies according to r and visual criteria applied to their spectroscopic properties between 3500 and 5300 Å.

We define three representative types:

- Sey2e: pure emission line spectra with only two stellar absorption features visible: Ca II K and G band and $r < 2$ ($EW([\mathrm{OIII}]\lambda5007) < -143$ Å);
- Sey2a: spectra showing both emission and absorption lines in which the Balmer series is not detected in absorption, even for the highest terms of the series and $r < 2$ ($EW([\mathrm{OIII}]\lambda5007) > -143$ Å);
- Sey2b: spectra for which the high order Balmer series is well detected in absorption and $r \geq 2$.

Spectra presented in Fig. A.1 belong to this latter sort.

5.4. Morphology versus star-forming activity

Storchi-Bergmann et al. (2000) suggested that Seyfert 2s with Balmer lines detected in absorption have preferentially a host galaxy of Hubble-type later than Seyfert 2s without Balmer lines. However, for this assertion, the authors used a new classification performed by Malkan et al. (1998). This classification could be seriously biased towards late Hubble-type galaxies since the spatial resolution reached with the HST and used for the classification is much higher than previous resolutions.

With our larger sample of 79 Seyfert 2 galaxies, we do not confirm this trend. Indeed, Fig. 9 shows that the distribution of Seyfert 2s with Balmer lines detected in absorption is very similar to the distribution of the whole sample. A Student's t test performed on both distributions indicated that the probability that both distributions are different is only 1%.

Subsample distributions are plotted in Figs. 5, 9, and 7.

6. Conclusions

We report here spectroscopic observations of 79 Seyfert 2 galaxies and 73 stars at a 2.2 Å resolution between 3500 and 5300 Å.

A general trend is found in the continuum slopes, in the sense that the external regions are much redder than the nuclei.

The nuclear spectra of the 79 Seyfert 2 galaxies can be put into one of three main types.

- Sey2e: only two stellar absorption features are seen (Ca II K and the G band) and the continuum slope tends to be the reddest.
- Sey2a: several stellar absorption features are visible but not the high order Balmer lines.
- Sey2b: strong high order Balmer lines are seen in absorption together with other stellar absorption features like Ca II K, CH and G bands. Young hot stars might be present in the nucleus and contribute significantly to the stellar light. In these galaxies, the continuum slope tends to be the flattest (bluest).

Considering only the 74 Seyfert 2 galaxies for which spectra have a good quality, one can group the galaxies into those three categories: we obtain 16 (22%) Sey2e galaxies, 21 (28%) Sey2a galaxies, and 37 (50%) Sey2b galaxies. Hence, at least half of the Seyfert 2 galaxies observed in this sample seems to harbour a young hot stellar population in their central region.

Such a trend has to be confirmed through a detailed spatial analysis of the stellar content in each galaxy in order to clearly disentangle nuclear and host components and estimate the physical properties (age, metallicity) of the stellar populations more accurately.

When considering distributions of Sey2b and Sey2e+a galaxies, we find no correlation between the host galaxy morphology and the stellar content of the central region. However, we observe a strong correlation between the level of featureless continuum and the detection of a young stellar population. This result favours the picture of a featureless continuum originated by the young stars themselves that would dilute the stellar absorption features formed by the older bulge component.

Acknowledgements. Authors are grateful to all the La Silla staff and especially the 2p2 team for generous and efficient supports during all these observing nights.

We thank the anonymous referee for precious suggestions which significantly improved the presentation of these results.

References

Allen, D. A., Norris, R. P., Meadows, V. S., & Roche, P. F. 1991, MNRAS, 248, 528

Aretxaga, I., Terlevich, E., Terlevich, R. J., Cotter, G., & Díaz, A. I. 2001, MNRAS, in press

Baldwin, J. A., Phillips, M. M., & Terlevich, R. 1981, PASP, 93, 5

Boisson, C., Joly, M., Moultaka, J., Pelat, D., & Serote Roos, M. 2000, A&A, 357, 850

Cardelli, J. A., Clayton, G. C., & Mathis, J. S. 1989, ApJ, 345, 245

Cayrel de Strobel, G., Soubiran, C., Friel, E. D., Ralite, N., & Francois, P. 1997, A&AS, 124, 299

Cid Fernandes, R. J., & Terlevich, R. 1995, MNRAS, 272, 423

Colina, L., Vargas, M. L. G., & Delgado, R. M. G. 1997, ApJ, 488, L71

Davoust, E., Paturel, G., & Vauglin, I. 1985, A&AS, 61, 273

Fairall, A. P., & Jones, A. 1991, Southern redshifts catalogue and plots (Publications of the Department of Astronomy, University of Cape Town, Cape Town: University, Department of Astronomy, 1991, 5th version)

Fitzgerald, M. P. 1970, A&A, 4, 234

González Delgado, R. M., Heckman, T., & Leitherer, C. 1998, ApJ, 505, 174

González Delgado, R. M., Heckman, T., & Leitherer, C. 2001, ApJ, 546, 845

Heckman, T., Krolik, J., Meurer, G., et al. 1995, ApJ, 452, 549
Heckman, T. M., González Delgado, R., Leitherer, C., et al. 1997, ApJ, 482, 114
Jacoby, G. H., Hunter, D. A., & Christian, C. A. 1984, ApJS, 56, 257
Joguet, B., Kunth, D., & Contini, T. 2001a, A&A, in preparation
Joguet, B., Terlevich, R. J., Kunth, D., Melnick, J., & Terlevich, E. 2001b, A&A, in preparation
Jones, L. 1997, Ph.D. Thesis (Chapel Hill: Univ. North Carolina)
Kurtz, M. J., & Mink, D. J. 1998, PASP, 110, 934
Leitherer, C., Alloin, D., Fritz-v. Alvensleben, U., et al. 1996, PASP, 108, 996
Lequeux, J. 2000, private communication
Lipovetsky, V. A., Neizvestny, S. I., & Neizvestnaya, O. M. 1988, Soobshcheniya Spetsial'noj Astrofizicheskoj Observatorii, 55, 5
Longhetti, M., Rampazzo, R., Bressan, A., & Chiosi, C. 1998, A&AS, 130, 251
Malkan, M. A., Gorjian, V., & Tam, R. 1998, ApJS, 117, 25
Mas-Hesse, J. M., & Kunth, D. 1991, A&AS, 88, 399
Nelson, C. H., & Whittle, M. 1995, ApJS, 99, 67
Pickles, A. J. 1985, ApJ, 296, 340
Rose, J. A. 1994, AJ, 107, 206
Schaerer, D., Contini, T., & Pindao, M. 1999, A&AS, 136, 35
Schmidt-Kaler, T. 1982, Numerical data and functional relationships in science and technology, new series, vol. 2b (Landolt-Börnstein), 31
Schmitt, H. R., Storchi-Bergmann, T., & Cid Fernandes, R. J. 1999, MNRAS, 303, 173
Silva, D. R., & Cornell, M. E. 1992, ApJS, 81, 865
Storchi-Bergmann, T., Raimann, D., Bica, E. L. D., & Fraquelli, H. A. 2000, ApJ, 544, 747
Taylor, B. J. 1999, A&AS, 134, 523
Terlevich, E., Diaz, A. I., & Terlevich, R. 1990, MNRAS, 242, 271
Tonry, J., & Davis, M. 1979, AJ, 84, 1511
Tran, H. D. 1995a, ApJ, 440, 565
Tran, H. D. 1995b, ApJ, 440, 578
Tran, H. D. 1995c, ApJ, 440, 597
Tüg 1976, The Messenger, 713
Vaceli, M. S., Viegas, S. M., Gruenwald, R., & de Souza, R. E. 1997, AJ, 114, 1345
Véron, M. P. 1981, A&A, 100, 12
Véron-Cetty, M., & Véron, P. 1998, ESO Sci. Rep., 18, 1
Véron-Cetty, M. P., & Véron, P. 2000, ESO Sci. Rep., 19, 1
Whitmore, B. C., McElroy, D. B., & Tonry, J. L. 1985, ApJS, 59, 1
Whittle, M. 1992, ApJS, 79, 49
Worthey, G., Faber, S. M., Gonzalez, J. J., & Burstein, D. 1994, ApJS, 94, 687